

Lab on a Chip

Accepted Manuscript



This is an *Accepted Manuscript*, which has been through the Royal Society of Chemistry peer review process and has been accepted for publication.

Accepted Manuscripts are published online shortly after acceptance, before technical editing, formatting and proof reading. Using this free service, authors can make their results available to the community, in citable form, before we publish the edited article. We will replace this *Accepted Manuscript* with the edited and formatted *Advance Article* as soon as it is available.

You can find more information about *Accepted Manuscripts* in the [Information for Authors](#).

Please note that technical editing may introduce minor changes to the text and/or graphics, which may alter content. The journal's standard [Terms & Conditions](#) and the [Ethical guidelines](#) still apply. In no event shall the Royal Society of Chemistry be held responsible for any errors or omissions in this *Accepted Manuscript* or any consequences arising from the use of any information it contains.

ARTICLE

The effects of 3D channel geometry on CTC passing pressure – towards deformability-based cancer cell separation

Cite this: DOI: 10.1039/x0xx00000x

Received 00th February 2014,
Accepted 00th May 2014

DOI: 10.1039/x0xx00000x

www.rsc.org/

Zhifeng Zhang¹, Jie Xu¹, Bin Hong², Xiaolin Chen¹

¹Mechanical Engineering, Department of ENCS, Washington State University, Vancouver, 98686, WA, USA

²TeloVISION, LLC, 1281 Win Henschel Blvd. West Lafayette, IN 47906, USA

Various lab on a chip devices have been developed recently to detect and separate circulating tumour cells (CTCs) for early stage cancer detection. Because CTCs are extremely rare in the blood, next generation CTC microfilters aim at significant improvement in both efficiency and throughput. CTC microfilters based on cell deformability seem to be a promising direction. In present research, we study CTC passing event through a micro filtering channel with various 3D geometries. The pressure signatures for different types of cells passing through different channels are characterized numerically. Specifically, five kinds of cross-sections, circular, square, triangular and two kinds of rectangular with aspect ratio of 2 and 5 are studied in this work. The total pressures for cell passing through the channels are calculated and reveal different behaviour from what is predicted by the static surface tension model. Among all five cross-sections studied, circular cross-section features the highest critical pressure, and thus is most suitable for high efficiency CTC separation. Square filtering channel provides the second largest critical pressure, and triangular cross-section provides the least critical pressure among these three cross-sections. All these three are better than rectangular channels with aspect ratio of 2 and 5. For rectangular channel, high aspect ratio channel may lead to cell splitting at high speed, which will result in periodic pressure signature. Our findings will provide valuable information for the design of next generation CTC microfilters.

Introduction

Cancer remains a major global health problem¹. Besides being locally invasive, cancer is known for its metastasizing capability. The metastatic cancer cells in the circulatory system are called Circulating Tumor Cells (CTCs). CTCs were first observed in the blood with metastasis in 1869. With advances in tumor biology and analytical technology, the unique seeding ability of CTCs was further

demonstrated for many types of tumors such as breast carcinoma, colon carcinoma, and malignant melanoma². With multiple physicochemical steps³, detached tumor cells could traverse the microenvironment and reach the blood vessels. After intravasation, CTCs could self-seed their tumors of origin or seed metastases in remote organs². Cancers are most likely operable and even curable if detected early and, therefore, early cancer detection offers substantial benefit to patients. Conventional methods for early cancer detection

mainly rely on medical imaging techniques¹ such as CT, X-ray, magnetic resonance imaging (MRI), thermal texture maps (TTM), and positron emission tomography (PET)⁴. However, these techniques are highly debatable in clinical practice for accurate cancer detection at early stage due to the uncertainty of these techniques by detecting abnormality instead of tumor as well as their side effects⁵.

CTCs are shed by the solid tumor and found to be a potential indicator for early tumor formation due to their presentation in the peripheral blood of cancer patients prior to that of clinical symptoms⁶. To detect CTCs, various methods have been developed⁶⁻⁸. Microfluidic devices, for instance, CTC microfilters⁹⁻¹⁰, have provided an easy, fast and accurate detection solution for non-invasive cancer diagnosis and close-to-real-time monitoring of cancer progression. Various cellular hallmarks can be employed for CTC detection in a CTC microfluidic device, and one category of label free CTC micro devices use cellular physical characteristics, such as size, deformability, acoustic properties¹¹ and dielectrophoretic features¹². Among all these physical characteristics, CTC microfilters based on cell deformability have the advantages of structural simplicity^{13,14}, stable performance and low cost¹⁵. For example, using channels, weirs¹⁴, pillars⁹, and membranes¹⁵, deformation-based CTC microfilters can auto-batch process blood purification or cancer cell capturing¹⁶. Most existing studies on deformation-based CTC microfilters focus on experimental tests based on static surface tension model. In order to achieve high capture efficiency, high isolation purity and high system throughput¹⁷, the CTC microfilters need to be optimized for the best geometry, which cannot be done if the complex cell/flow/channel interactions are not fully understood. Numerical simulation can be a powerful tool for studying the cell behaviour inside a filtering channel. For example, previous models have explored the entry channel pressure influence¹⁷⁻¹⁹ and entrance time¹⁸. However, to the best of our knowledge, the performance of 3D channel geometries on the deformation of CTC remains elusive in the literature.

Various models are developed using either the micro/nanostructural approach or the continuum approach. The former was developed to investigate the contribution of the cell membrane and cytoskeleton to the mechanical behaviours of suspended cells²⁰⁻²³. The latter treats the cell as comprising materials with certain continuum material properties²⁴. Although providing less insight into the detailed interactions at the subcellular level, the continuum approach is easier and more straightforward to use in modelling the cell/fluid/channel interaction if the effective mechanical response at the cell level is all that is needed as in the case of filtering process. The continuum approach can be categorized into liquid or solid models^{19, 20}. By considering the cell as a liquid droplet, the liquid model uses the governing equations consisting of mass and momentum balance for both the cell and the surrounding flow, and is generally considered to perform better than solid models for large deformation problems^{7,18}.

In present research, we explore key parameters such as pressure behaviour and velocity influence under various 3D geometries of a CTC filtering channel. Cell fluid model is employed for proper

treatment of the large deformation of cells^{7,18}. The deformability of CTC and inlet pressure is numerically simulated by Volume of Fluid (VOF) algorithm²⁵. We first study the behaviour of CTC and white blood cells when they are pushed through a micrometre sized filtering channel. These channels feature uniform lengthwise cross-section with various cross-sectional shapes. The pressure signatures of cell passing these filtering channels are described under constant flow rate. Surface tension terms obtained in present paper are compared with quasi-static Young-Laplace surface tension model for different geometries. The discrepancies between our results and the Young-Laplace model are interpreted via detailed cell deformation analysis. These data and analyses will provide useful insight for future development of high efficiency CTC microfilters.

Model Description

When the blood flows through a filtering channel in a microfluidic chip, the more deformable normal blood cells can simply flow or squeeze through but the stiffer CTCs will be blocked. The critical channel diameter is reported to be within 5-12 μm for effective filtering of CTCs according to different cell sorting methods^{14,26}. In this study, we use a circular channel with a diameter of 5 μm as baseline geometry. Fig.1 shows an illustration of the circular channel design.

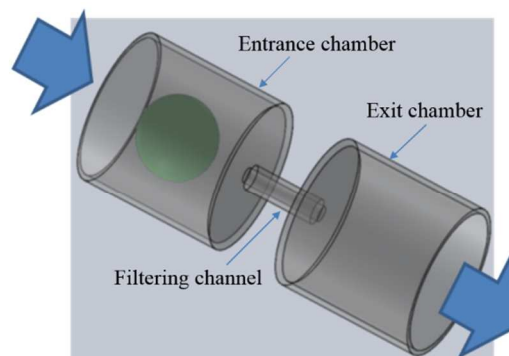


Fig. 1 Mechanical model for cell passing a filtering channel.

Both CTCs and normal blood cells vary significantly in size and deformability²⁷⁻²⁹. One consistent finding has been observed that CTCs are typically larger and stiffer than normal blood cells although malignant CTCs with increased metastatic potential tend to have increased deformability^{30, 31}. Considering the extremely heterogeneous CTC population, deformability-based microfilter is capable of targeting the largest possible subset of CTC population compared with the conventional antibody approach which targets only certain subpopulations of CTCs. For convenience, typical cell properties that fall within the reported range have been used in our model. For example, the surface tension of a CTC^{13, 32, 33} and a white blood cell²⁹ is considered to be 50×10^{-3} and 30×10^{-6} N/m respectively. The cell deformation is described using the fluid model of a droplet bounded by surface tension. Note that, the red blood cells are neglected in our model, since they are small and highly

deformable to pass any filtering channel within normal design range.

Theoretical Background

The total inlet pressure P_t during a cell passing through a channel is mainly used to overcome two types of resistance, 1) viscous resistance; 2) resistance caused by surface tension, which acts to preserve the integrity of the cell surface:

$$P_t = P_{vis} + P_{sur} \quad (1)$$

Pressure drop due to viscosity (P_{vis})

For pressure driven flow, the viscous resistance is caused by fluid viscosity which can be summarized by the Hagen-Poiseuille law³⁴,

$$P_{major} = R_{hyd} \times Q_V \quad (2)$$

where P_{major} is the viscous pressure drop of the channel. R_{hyd} is the hydraulic resistance. Q_V is the volume flow rate. For different cross-sections, the hydraulic resistance R_{hyd} is different.

Due to constriction from the inlet of the filtering channel and the expansion from the exit of the filtering channel, minor pressure drop P_{minor} exists and can be calculated by the following equation,

$$P_{minor} = K_C \frac{\rho V^2}{2} + K_E \frac{\rho V^2}{2} \quad (3)$$

where V is the flow velocity in the filtering channel. K_C is constriction coefficient and K_E is expansion coefficient. K_C is selected to be 0.5 and $K_E = 1$ assuming the filtering channel is much smaller than the outside chambers.

Pressure drop due to surface tension (P_{sur})

The surface tension-geometry relation can be treated using the cortical shell-liquid core model. The model uses a quasi-static Young-Laplace relation, which predicts a critical pressure needed for a cell to be squeezed into a filtering channel as following,

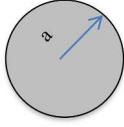
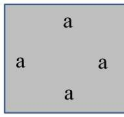
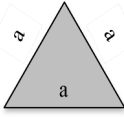
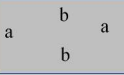
$$P_{sur} = 2\sigma \left(\frac{1}{R_{channel}} - \frac{1}{R_{cell}} \right) \quad (4)$$

Here, σ is the surface tension coefficient; $R_{channel}$ is the radius of a circular filtering channel, and R_{cell} is the radius of main cell body. This model is successfully used in micropipette aspiration experiments to evaluate the surface tension of cells³⁵. The model is based on a near-static process, and has been widely used for CTC microfilter design. Based on the Young-Laplace analysis, the critical pressure for a non-circular channel is given by³⁴,

$$P_{sur} = \sigma \cos(\theta) \left(\frac{C_{pw}}{A_p} - \frac{2}{R_{cell}} \right) \quad (5)$$

C_{pw} is the wet perimeter of cross-section; A_p is the area of cross-section, and θ is the contact angle between the cell and fluid media (180° for our model). In present study, we will compare our numerical results to this Young-Laplace relation, and show its shortcomings for dynamic flow conditions and non-circular geometries.

Table 1 Designed geometries and their critical pressures for a CTC

Cross-section shapes of the filtering channel	Hydraulic resistances R_{hyd}	Key dimensions based on a constant P_{vis} (μm)	Critical pressure expression P_{sur}	Critical P_{sur} value (kPa)
Circular 	$\frac{8}{\pi} \eta L \frac{1}{a^4}$	a=2.50	$2\sigma \cos(\theta) / a - \frac{2\sigma}{R_{cell}}$	27.5
Square 	$28.4 \eta L \frac{1}{a^4}$	a=4.57	$4\sigma \cos(\theta) \left(\frac{1}{a} \right) - \frac{2\sigma}{R_{cell}}$	31.26
Triangular 	$\frac{320}{\sqrt{3}} \eta L \frac{1}{a^4}$	a=7.30	$12\sigma \cos(\theta) / \sqrt{3} a - \frac{2\sigma}{R_{cell}}$	34.95
Rectangle 	$\frac{12}{1 - 0.63(a/b)} \eta L \frac{1}{a^3 b}$	$\beta = b/a = 2,$ a=3.41 and b=6.82	$2\sigma \cos(\theta) \left(\frac{1}{a} + \frac{1}{b} \right) - \frac{2\sigma}{R_{cell}}$	31.49
		$\beta = b/a = 5,$ a=2.55, b=12.75		34.55

A summary of the pressure calculations of a CTC microfilter with various channel shapes is tabulated in Table 1. Five different cross-sections are studied, circular, square, triangular and two rectangular channels with aspect ratio of 2 and 5. For meaningful comparison of these shapes, we fixed the value of P_{vis} at a constant using the circular channel as a baseline, and calculated the dimensions of all other shapes.

Numerical method

The transient simulation of a cell passing through a filtering channel is performed using commercial software ANSYS Fluent. The Volume of Fluid (VOF) method is employed to track the interface between the cell and its surrounding medium. Explicit time stepping scheme is used with the Courant number set within 0.5-5 to ensure that the scheme is both stable and convergent. The cell-water interface is reconstructed using the Geo-reconstruct scheme available in Fluent. The channel walls are set as no-slip and stationary.

Inflation layers are used to achieve accurate resolution of the boundary layer. The 3-D mesh is inflated along the wall regions of the narrow channel where the cell is passing through. For the circular channel, a 2-D axisymmetric model is employed, and the mesh is inflated along the symmetry line as well as the walls of the narrow channel. The total number of elements used for the 3-D simulation is around 200,000, with nearly 5000 elements patched for the cell. Both CTCs and white blood cells are assumed incompressible.

The VOF method³⁶ is based on the fact that the two phases form an impenetrable interface, which can be easily understood as the membrane of a cell. The method is achieved through the volume fraction of a primary phase (α), which varies between 0 and 1. An example of how the primary-phase volume fraction varies near the interface is illustrated schematically in Fig. 2.

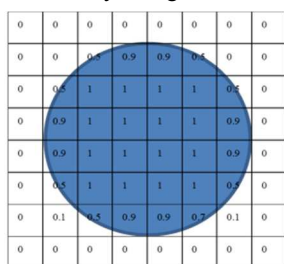


Fig. 2 Values of the volume fraction for each of the phases and the interface ($\alpha=1$ in cell, $\alpha=0$ in water, $0<\alpha<1$, at interface)

The interface is tracked by solving the transport equation for the primary-phase volume fraction. Assuming no mass transfer between the two phases, the continuity equation can be written as,

$$\frac{\partial \alpha}{\partial t} + \nabla \cdot (\alpha \vec{V}) = 0 \quad (6)$$

Here \vec{V} is the velocity vector. According to Eq (6), the substantial derivative of the primary-phase volume fraction is zero so that the interface-tracking is achieved through the velocity field at the interface.

The following momentum equation is solved for the whole computational domain and the velocity field is shared between the two phases:

$$\frac{\partial}{\partial t} (\rho \vec{V}) + \nabla \cdot (\rho \vec{V} \vec{V}) = -\nabla p + \nabla \cdot [\mu (\nabla \vec{V} + \nabla \vec{V}^T)] + \rho \vec{g} + \vec{F} \quad (7)$$

Where \vec{g} is the gravitational acceleration vector and \vec{F} is the source term. In the two-phase flow, surface tension force contributes to the source term. ρ and μ are volume-fraction-averaged density and viscosity, respectively. The material properties are determined by considering the volume fraction of each phase in a control volume. For the two phase flow, e.g., the volume-fraction-averaged density can be given as follows:

$$\rho = \alpha \rho_2 + (1 - \alpha) \rho_1 \quad (8)$$

Here ρ_2 is the density of cell while ρ_1 is the density of water. Using the divergence theorem, the surface tension force, i.e., the source term added to the momentum equation, is given by,

$$\vec{F}_{vol} = \sigma \frac{2\rho\kappa\nabla\alpha}{(\rho_1+\rho_2)} \quad (9)$$

Where σ is the surface tension coefficient between cell and water, κ is the mean curvature of the interface in the control volume.

The curvature of the surface near the wall is adjusted by imposing the so-called dynamic boundary condition and considering the effect of static contact angle as follows:

$$n_i = n_w \cos(\theta_{st}) + n_t \sin(\theta_{st}) \quad (10)$$

Where n_w is the unit vector normal to the wall, n_i is a vector on the wall and normal to the contact line, and θ_{st} is the static contact angle. In present study, the static contact angle is selected as 180° for phase interaction.

Results and discussion

Pressure analysis

When a cell is passing through a filtering channel at a constant speed, the pressure in the channel will first increase and then decrease. The maximum pressure occurs when the cell is entering into the filtering channel and the minimum pressure occurs when the cell is exiting the channel. This maximum pressure is therefore the critical pressure to ensure a successful passing event of a cell. In practical CTC microfilters, the flow is often driven by pressure. Therefore, for successful CTC separation, the operating pressure of the device needs to be kept below the critical pressure of a CTC and above the critical pressure of normal blood cells. As mentioned before, this inlet pressure is used for balancing two types of resistances, and can be decomposed into P_{vis} and P_{sur} . In this section, we first verify this concept by studying the influence of the flow velocity on the inlet pressure P_t for a circular channel. As can be seen from Fig. 3, the inlet pressure P_t for a CTC to pass through a circular channel increases with increasing flow velocity. At the same time, the P_{vis} also increases at the roughly the same speed with increasing velocity. Simulation results match well with

theoretical P_{vis} calculated from Eq. 2 and Eq. 3. It is therefore evident that the increase in the inlet pressure at high flow rate is mainly due to the viscous resistance in the channel, while the P_{sur} is relatively constant. Similar results can be obtained for other geometry cross-sections. For comparison purpose, we fixed the viscous pressure for all the following studies at 7.9 kPa by fix the flow rate at 7 (nL/s) (unless otherwise noted).

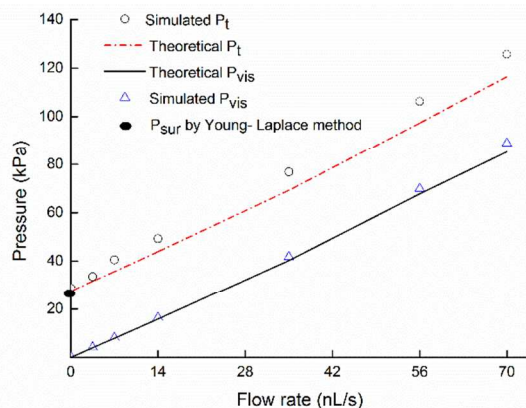


Fig. 3 The effect of flow rate on pressure components when cancer cell passes a circular channel.

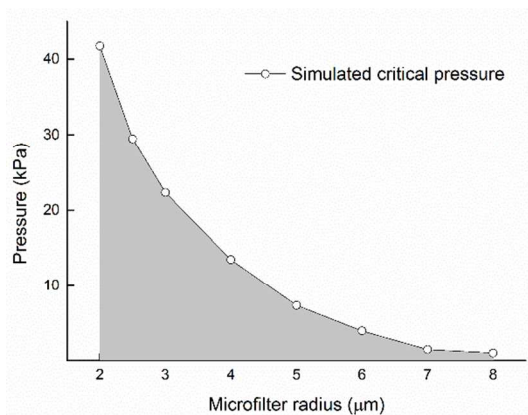


Fig. 4 Microfilter size effect on the critical pressure.

We next investigate the influence of the filter hole size on the critical pressure of CTC passing a circular channel. As can be seen from Fig.4, the simulated critical pressure of CTC passing through a circular channel decreases with the increasing microfilter radius. According to the modelling of the filtering process, a CTC fails to pass through the filter when the inlet pressure is less than the corresponding critical pressure for a given filter size. The shaded area in Fig. 4 provides conditions that the CTC cannot pass through the filter.

Fig. 5 plots the pressure profiles of cells passing through different filtering channels. As can be seen from Fig 5, at the same viscous pressure P_{vis} , the filtering channel with circular cross-section requires the highest inlet pressure P_t for a CTC to pass through. Square channel produces the second largest pressure followed by the

triangular filtering channel. All these three geometries are better than rectangular filtering channels with $\beta=2$ and 5. Since the higher inlet pressure P_t means the easier to separate a CTC from normal blood cells, we can rank the channel performance according to the predicted critical pressure: circular > square > triangular > rectangular ($\beta=2$) > rectangular ($\beta=5$). Here, we introduce the concept of roundness of geometry to assist our comparison:

$$\text{Roundness} = \frac{4\pi A_p}{C_{AP}^2} \quad (11)$$

Where A_p is the cross sectional area and C_{AP} is the perimeter of the cross-section. Understandably, the roundness of a circular shape is 1 and the more deviation from the circular shape, the smaller roundness value will be. The calculated roundness values of our studied cross-sectional shapes are listed in Fig. 6, and plotted with the critical pressures for CTC filtering obtained from simulations. As can be seen from Fig 6, with the decrease in roundness, the pressure needed to separate the cancer cell will also decrease. In Fig. 6, we also plotted the critical pressures calculated from the classical quasi-static Young-Laplace model (see the last column in Table 1), which indicates a reverse trend, i.e., the critical pressure increases with increasing roundness. Therefore, it is precarious to apply the classical model for the design of CTC microfilters, since no dynamic effects are considered in the model. For example, the main assumption for the classical is that the cell can fully occupy the channel cross-section area, while our simulation shows that the cells did not fill up the entire channel cross section if there are sharp corners, which may induce leakage flow through the channel from inlet to outlet. This issue is discussed in greater detail in the next section.

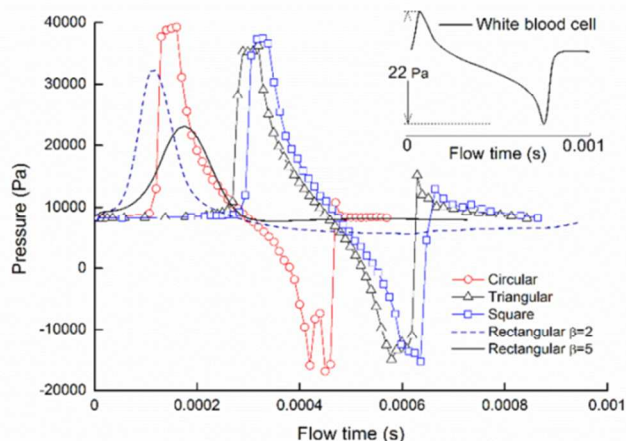


Fig. 5 Pressure signatures of CTC and white blood cells when they are passing through various 3D cross-sections at a constant flow rate. The y-axis is the inlet pressure measured P_t in the simulation. White blood cells produce a negligible pressure drop which is magnified in the inset.

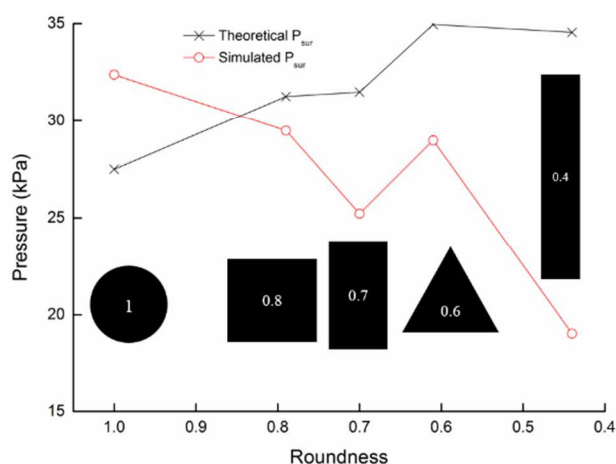


Fig. 6 The relation between the critical pressures and the channel cross-section roundness – comparison between theory and simulation.

The effects of cell deformation

As can be seen in Fig. 7, the CTC deforms significantly when entering a filtering channel due to the channel constriction.

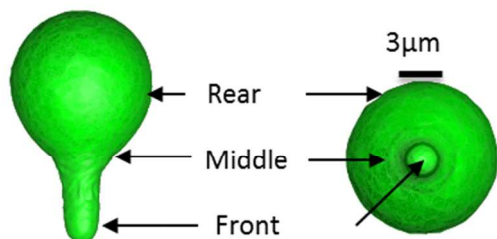


Fig. 7 Typical deformation of a CTC when entering a circular filtering channel. The channel is made invisible to aid the cell visualization.

Fig. 8 compares the deformation of a CTC and a white blood cell when they are inside a circular filtering channel. We can see that the CTC can fully fill the channel while the white blood cell shares the channel with the surrounding fluid. Another observation is that, the front and rear parts of the cancer cell that are outside the channel is nearly spherical in shape, while the white blood cell shows a more streamlined shape.

We can analyse the deformation using capillary number³⁷ (Ca). Ca number has been used to study biology cells¹⁸, which is defined as $Ca = \mu V / \sigma$. It is the ratio of viscous force and surface tension force. The Ca number for a white blood cell in the studied case is approximately 1, which means that the surface tension force is comparable to the viscous force³⁸. At the same velocity, Ca number for a CTC is about 6×10^{-3} , meaning that surface tension force governs the cancer cell deformation, which can explain why the cancer cell maintains a spherical shape easily and can fill the entire channel.

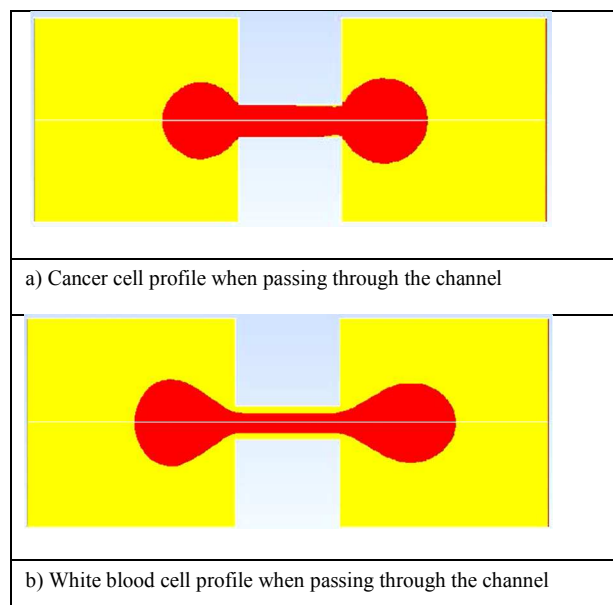


Fig. 8 Deformation of a cancer cell and a white blood cell when they are passing through a filtering channel.

The whole process of pressure change during cell passing through a circular filtering channel is demonstrated in Fig. 9. In stage a, cancer cell has not reached the filtering channel yet, and the pressure is nearly constant. The cell deformation is negligible at stage a.

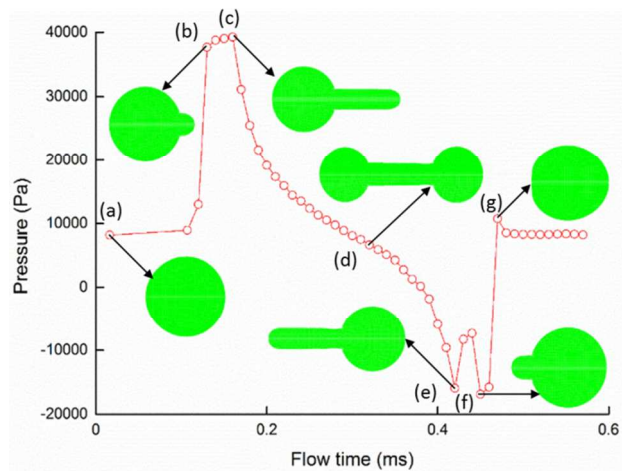


Fig. 9 Pressure-deformation relation of a cancer cell. Stages are, a) initial state, b) maximum pressure begins, c) maximum pressure finishes, d) pressure balanced and equals to background pressure, e) minimum pressure begins, f) minimum pressure stage finished, g) rear part bouncing.

After initial deformation, the cell goes through very quick deformation to the critical pressure at stage b. The front part deforms into a near half spherical convex. With continuous pushing from fluid flow, this convex front will be finally squeezed into the channel. Between stage b and stage c, pressure maintains at the high level,

Lab on a chip

when the cancer cell goes through huge deformation to pass through the channel from $16\mu\text{m}$ sphere a to $5\mu\text{m}$ cylinder-like shape. After stage c, cell begins to come out of the filtering channel on the other side. As soon as the front part of the cell moves out of the channel, its radius of curvature starts to increase. Meanwhile, the back part of the cell keeps shrinking to produce smaller and smaller radius of curvature. Therefore, the net surface tension resistance force of the cell starts to decrease. At a point d, both ends of the cell are equal in size and the net surface tension force reduces to zero, and in turn, the inlet pressure shown in the figure reaches the pure viscous pressure level. After this tipping point, the net surface force changes its direction and actually pulls the cell out of the channel, which causes the decrease in the fluid pressure.

After the cell moves out entirely from the filtering channel, we notice that the rear part of the cell may go through a rebound process forming a slight concave at stage g. This should be due to fluid inertia. The concave-shaped deformation is more obvious at higher velocity.

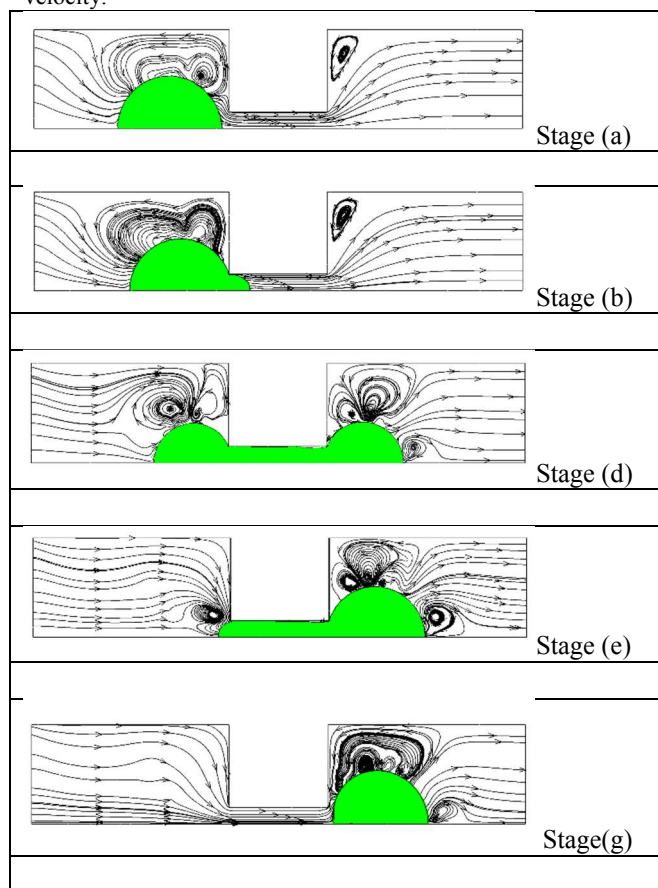


Fig. 10 Streamline of CTC passing microfilter at different stages.

The streamlines inside the microfilter induced by a cell passing through at different stages are shown in Fig 10. Due to the blockage of cell, the flow has to increase its speed in the small gap between the cell and the wall. A pressure difference is generated across the cell which drags the cell into the filter. The cell follows underlying fluid streamlines in the

microfilter, and recovers its spherical shape by the surface tension effect after passing through the microfilter.

We also compared the deformation of cells in several non-circular channels as shown in Fig. 11. One major difference is that cell could not fully fill the channel as it does in the circular channel case. Therefore, the use of Young-Laplace equation in Table 1 will definitely involve errors.

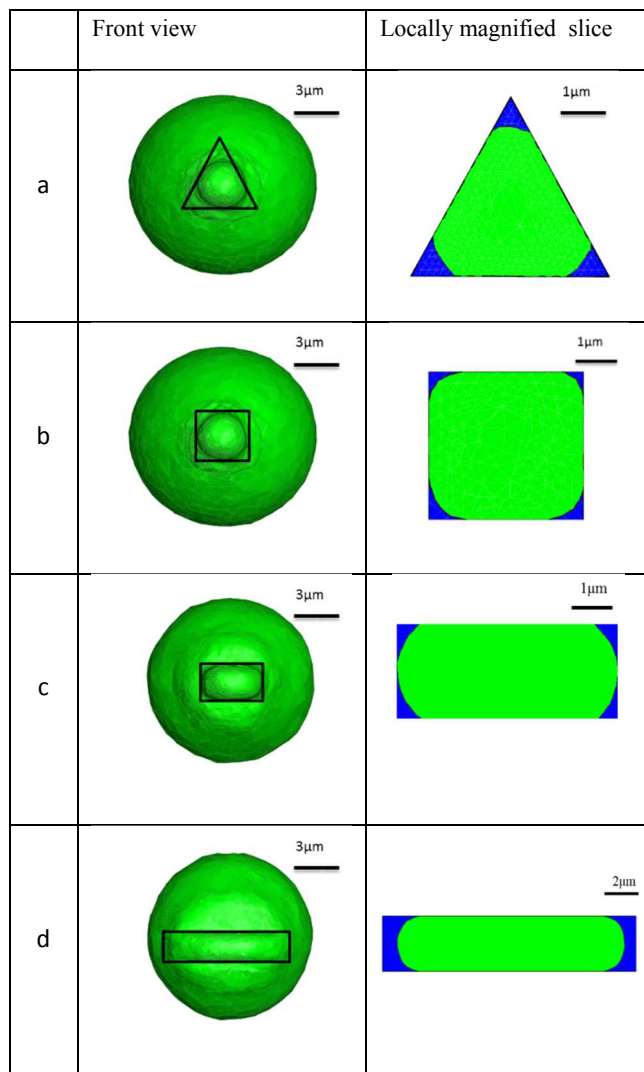


Fig. 11 Cell deformation for 3D filtering channel at the critical pressure point, a) triangular case; b) square case; c) rectangular case with $\beta=2$; d) rectangular case with $\beta=5$.

As can be seen that at the entrance of triangular filtering channel, the centre part is occupied by the cancer cell, and the corners near three vertices are filled by the surrounding fluids. The same situation happens for all other 3D geometries. We can also see that if the aspect ratio of the rectangular channel increases, the fluids will occupy more space inside the filtering channel. Another interesting observation for a large aspect ratio channel is that cells can split into smaller parts as illustrated in

Fig. 12. Cell splitting is a nonlinear phenomenon³⁹ for droplet model. It has a strong correlation with channel geometry and flow velocity. Detached daughter cells are reported in a similar droplet dispenser device. For theoretical study, the splitting phenomenon was reported to have relation with Ca number and shear stress^{40, 41}.

studied. High aspect ratio rectangular channel may lead to cell splitting at a high speed, which will result in periodic pressure signature. Our findings will aid in the design of next generation CTC microfilters by offering insight into the role that 3D channel geometry plays in deformation-based CTC separation.

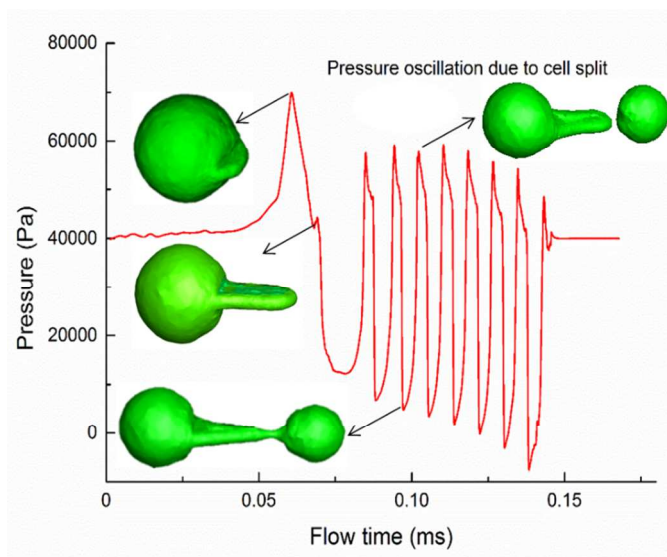


Fig. 12 Pressure oscillation due to cell split for high aspect ratio channel ($\beta=5$). Inlet velocity is selected as 0.05 (m/s).

In present study, cell splitting for circular, triangular, square and rectangular with $\beta=2$ are not observed under the studied parameters. However, for the higher aspect ratio rectangular channel with $\beta=5$, the CTC splits at the outlet. The ruptured daughter cells will merge, and keep splitting and merging until they both pass through the hole. The cell merging results from the lack of cell membrane in our droplet model. The cell split is due to the surface-tension-driven Rayleigh-Plateau instability⁴² with main source of perturbation coming from the anisotropic elongation of the cell body at the exit of the rectangular channel⁴³. Lowering the fluid speed will prevent the cell from splitting, which agrees with a previous numerical study³⁹.

Conclusions

CTC passing event through a 3D micro filtering channel is studied in this work. The pressure signatures for different types of cells passing through different channels are characterized numerically. The effect of 3D channel geometry on the total pressure for cell passing through the channels is examined. Among the five cross-sections studied, circular cross-section features the highest critical pressure, and thus is most suitable for high efficiency CTC separation. As the cross-section deviates from a round shape, the pressure needed to separate the cancer cell decreases with decreasing roundness of the cross-section. Between the two equilateral polygon cross-sections, the square filtering channel provides a larger critical pressure than that of the triangular channel. The rectangular channels provide the least critical pressures among all the different cross-sections

Reference

- P. Boyle and B. Levin, *World cancer report 2008*, IARC Press, International Agency for Research on Cancer, 2008.
- M.-Y. Kim, T. Oskarsson, S. Acharyya, D. X. Nguyen, X. H.-F. Zhang, L. Norton and J. Massague, *Cell*, 2009, **139**, 1315-1326.
- P. Koumoutsakos, I. Pivkin and F. Milde, in *Annual Review of Fluid Mechanics, Vol 45*, eds. S. H. Davis and P. Moin, Annual Reviews, Palo Alto, 2013, vol. 45, pp. 325-355.
- S. S. Gambhir, *Nature Reviews Cancer*, 2002, **2**, 683-693.
- D. E. Midthun, *Clinical Update*, 2012, **28**, 1-3.
- B. Hong and Y. Zu, *Theranostics*, 2013, **3**, 377-396.
- F. Fabbri, S. Carloni, W. Zoli, P. Ulivi, G. Gallerani, P. Fici, E. Chiadini, A. Passardi, G. L. Frassinetti and A. Ragazzini, *Cancer letters*, 2013, **335**, 225-231.
- C. Alix-Panabières and K. Pantel, *Lab on a Chip*, 2014, **14**, 57-62.
- S. Nagrath, L. V. Sequist, S. Maheswaran, D. W. Bell, D. Irimia, L. Utkus, M. R. Smith, E. L. Kwak, S. Digumarthy and A. Muzikansky, *Nature*, 2007, **450**, 1235-1239.
- S. Zheng, H. K. Lin, B. Lu, A. Williams, R. Datar, R. J. Cote and Y.-C. Tai, *Biomedical microdevices*, 2011, **13**, 203-213.
- X. Ding, S.-C. S. Lin, M. I. Lapsley, S. Li, X. Guo, C. Y. Chan, I.-K. Chiang, L. Wang, J. P. McCoy and T. J. Huang, *Lab on a Chip*, 2012, **12**, 4228-4231.
- A. B. Fuchs, A. Romani, D. Freida, G. Medoro, M. Abonnenc, L. Altomare, I. Chartier, D. Guergour, C. Villiers and P. N. Marche, *Lab on a Chip*, 2006, **6**, 121-126.
- S. M. McFaul, B. K. Lin and H. Ma, *Lab on a chip*, 2012, **12**, 2369-2376.
- H. Mohamed, M. Murray, J. N. Turner and M. Caggana, *Journal of Chromatography A*, 2009, **1216**, 8289-8295.
- D. R. Gossett, W. M. Weaver, A. J. Mach, S. C. Hur, H. T. K. Tse, W. Lee, H. Amini and D. Di Carlo, *Analytical and bioanalytical chemistry*, 2010, **397**, 3249-3267.
- E. Sollier, D. E. Go, J. Che, D. R. Gossett, S. O'Byrne, W. M. Weaver, N. Kummer, M. Rettig, J. Goldman and N. Nickols, *Lab on a Chip*, 2014, **14**, 63-77.
- T. J. Huang, *Lab on a Chip*, 2013, **13**, 602-609.
- F. Y. Leong, Q. Li, C. T. Lim and K.-H. Chiam, *Biomechanics and modeling in mechanobiology*, 2011, **10**, 755-766.
- T. Secomb and R. Hsu, *Biophysical journal*, 1996, **71**, 1095-1101.
- Z. Peng, X. Li, I. V. Pivkin, M. Dao, G. E. Karniadakis and S. Suresh, *Proceedings of the National Academy of Sciences*, 2013.
- J. B. Freund, *Annual Review of Fluid Mechanics*, 2014, **46**, 67-95.
- S. K. Boey, D. H. Boal and D. E. Discher, *Biophysical Journal*, 1998, **75**, 1573-1583.
- J. Li, M. Dao, C. Lim and S. Suresh, *Biophysical Journal*, 2005, **88**, 3707-3719.
- C. Lim, E. Zhou and S. Quek, *Journal of Biomechanics*, 2006, **39**, 195-216.
- J. D. Anderson, *Computational fluid dynamics*, McGraw-Hill New York, 1995.
- M. Gusenbauer, I. Cimrak, S. Bance, L. Exl, F. Reichel, H. Oezelt and T. Schrefl, *arXiv preprint arXiv:1110.0995*, 2011.
- I. Sokolov, *Cancer Nanotechnology*, 2007, 1-17.
- M. J. Rosenbluth, W. A. Lam and D. A. Fletcher, *Biophysical journal*, 2006, **90**, 2994-3003.
- J. D. Bronzino, *The biomedical engineering handbook*, CRC press Boca Raton, FL, 1995.
- R. A. Harouaka, M. Nisic and S.-Y. Zheng, *Journal of laboratory automation*, 2013, **18**, 455-468.
- S. Byun, S. Son, D. Amodei, N. Cermak, J. Shaw, J. H. Kang, V. C. Hecht, M. M. Winslow, T. Jacks and P. Mallick, *Proceedings of the National Academy of Sciences*, 2013, **110**, 7580-7585.
- A. Preetha, N. Huilgol and R. Banerjee, *Biomedicine & pharmacotherapy*, 2005, **59**, 491-497.
- Q. Guo, S. M. McFaul and H. Ma, *Physical Review E*, 2011, **83**, 051910.
- H. Bruus, *Theoretical microfluidics*, Oxford University Press, 2008.
- R. M. Hochmuth, *Journal of Biomechanics*, 2000, **33**, 15-22.
- T. Darvishzadeh and N. V. Priezjev, *Journal of Membrane Science*, 2012.
- P.-G. De Gennes, F. Brochard-Wyart and D. Quéré, *Capillarity and wetting phenomena: drops, bubbles, pearls, waves*, Springer, 2004.
- X. Hu, A. Salsac and D. Barthès-Biesel, *Journal of Fluid Mechanics*, 2012, **705**, 176-194.
- S. Protière, M. Z. Bazant, D. Weitz and H. Stone, *Europhysics Letters*, 2010, **92**, 54002.
- C. Chung, M. Lee, K. Char, K. H. Ahn and S. J. Lee, *Microfluidics and nanofluidics*, 2010, **9**, 1151-1163.
- C. Chung, K. H. Ahn and S. J. Lee, *Journal of Non-Newtonian Fluid Mechanics*, 2009, **162**, 38-44.
- A. S. Utada, A. Fernandez-Nieves, J. M. Gordillo and D. A. Weitz, *Physical review letters*, 2008, **100**, 014502.
- D. Saeki, S. Sugiura, T. Kanamori, S. Sato, S. Mukataka and S. Ichikawa, *Langmuir*, 2008, **24**, 13809-13813.